Applied Magnetic Resonance (2022) 53:1089–1104
https://doi.org/10.1007/s00723-021-01424-0

Applied
Magnetic Resonance

ORIGINAL PAPER

Local Environment of Superoxide Radical Formed on the TiO_2 Surface Produced From $Ti(OiPr)_4$ Exposed to H_2O_2

Rimma I. Samoilova[1] · Sergei A. Dikanov[2]

Received: 28 April 2021 / Revised: 15 August 2021 / Accepted: 27 August 2021 /
Published online: 17 September 2021

Abstract

A selective heterogeneous catalyst with the superoxide anion $O_2^{\bullet-}$ stable at room temperature, generated by treating $Ti(OR)_4$ (R = iPr, nBu) with H_2O_2, was previously reported and used for the oxidation of organic compounds. It was proposed that exceptional stability of the $O_2^{\bullet-}$ is resulted from its stabilization near Ti^{+4} cation on the TiO_2 surface with the participation of water molecules and/or OH groups. In this article, we performed high-resolution pulsed EPR study on the $O_2^{\bullet-}$ in this catalyst with the aim to obtain quantitative information about its interactions with the surrounding molecules. Our data has shown that the $O_2^{\bullet-}$ is involved in weak hyperfine interactions with protons in the nearest environment, which do not exceed a value of 2 MHz. It corresponds to an O_s…H distance of ≥ 3 Å that excludes the formation of hydrogen bonds. The analysis of possible structures of $O_2^{\bullet-}$ adsorption on TiO_2 surface taking into account our results and lack of radical mobility at room temperature previously observed in EPR spectra led us to suggest that the $O_2^{\bullet-}$ is stabilized in the form of superoxo bridge coordinated with two titanium atoms.

1 Introduction

Superoxide anion ($O_2^{\bullet-}$) is a radical species formed as a result of the one-electron reduction of dioxygen (O_2), which occurs in different chemical and biological systems [1]. Studies of the superoxide radical reactions with organic compounds have shown that it can behave as a base, a nucleophile, and an oxidizing or reducing agent [2, 3]. The generation of $O_2^{\bullet-}$ was achieved by electrolytic reduction, enzymes, or

✉ Sergei A. Dikanov
dikanov@illinois.edu

[1] Voevodsky Institute of Chemical Kinetics and Combustion, Russian Academy of Sciences, Novosibirsk 630090, Russian Federation

[2] Department of Veterinary Clinical Medicine, University of Illinois at Urbana-Champaign, Urbana, IL 61801, USA

using a photoinduced electron-transfer process. Since superoxide anion is paramagnetic, the broad application of multifrequency, continuous-wave EPR spectroscopy can be applied for its detection and characterization in chemical and biological systems [4–8]. Particularly, the formation of superoxide ion on the surfaces of oxides (MgO/CaO, ZnO, ZrO_2, and TiO_2) was observed in electron transfer processes initiated by photoexcitation or radiation [4]. These photocatalytic reactions are successfully used for the synthesis and purification of water effluents from toxic organic substances. The treatment of an oxide with a solution of hydrogen peroxide (H_2O_2) followed by drying the solid under vacuum has also been proposed to generate superoxide radicals [9].

A catalyst with matrix-bound superoxide anion, generated by treating $Ti(OR)_4$ (R = iPr, nBu) with H_2O_2, was reported and used as a selective heterogeneous catalyst for the oxidation of organic compounds [10]. The catalyst is effective even at room temperatures and with various solvents including water. Its detailed study using different spectroscopic techniques (FTIR, EPR and Raman) as well as X-ray diffraction (XRD), thermogravimetric/differential and elemental analysis has led to the conclusion that the particle responsible for the reaction was superoxide radical. These studies also suggest that the exceptional stability of the radical is resulted from its location near Ti^{+4} cation on the TiO_2 surface with the participation of water molecules and/or OH groups [10–14]. Despite this conclusion, the nature and strength of $O_2^{\bullet -}$ interactions with the surrounding molecules remain unknown and the quantitative characterization of the environment for the trapped superoxide was not described.

In this work, the stabilization of paramagnetic intermediates during decomposition of hydrogen peroxide on the TiO_2 surface has been studied using pulsed X and Q-band EPR spectroscopy. We used high-resolution pulsed EPR techniques, i.e. 1D and 2D ESEEM and ENDOR, to resolve weak interactions of the unpaired electron of the superoxide with the surrounding magnetic nuclei and to discuss the model of the superoxide environment using quantitative data about these interactions.

2 Experimental Section

TiO_2/superoxide catalyst was prepared according to the method described in [10], i.e. 30% H_2O_2 (5.98 g, 0.175 mol) was added slowly to a solution of $Ti(OiPr)_4$ [titanium (IV) isopropoxide $Ti(OCH(CH_3)_2)_4$, *m*, *w*. 284.22] (5.0 g, 0.0175 mol) in anhydrous CH_3OH (50 mL) over 40 min under N_2 with stirring at room temperature. The yellow precipitate that formed was collected by filtration on a sintered funnel, washed with anhydrous methanol, and dried under reduced pressure (3 mmHg) at 25° C for 1 h for complete removal of the solvent from TiO_2 dispersion (sample I). Obtained powder was transferred into quartz X and Q-band EPR tubes, degassed and sealed. There is only one difference with [10] in the preparation of the catalyst. We used commercially available 30% H_2O_2 instead of 50% in [10]. Similar samples were analogously prepared using D_2O_2. Deuterated hydrogen peroxide was obtained by repeating twice the evaporation procedure to 1/3 volume of the mixture 0.311 g D_2O and 0.316 g 30% H_2O_2.

The pulsed EPR experiments were carried out using an X and Q-band Bruker ELEXSYS E580 spectrometer equipped with Oxford CF 935 cryostats. Several types of experiments with different pulse sequences were employed with appropriate phase-cycling schemes to eliminate unwanted features from the experimental echo envelopes. Among them are two-pulse and four-pulse sequences. In the two-pulse experiment ($\pi/2 - \tau - \pi - \tau -$ echo), the intensity of the echo signal is measured as a function of the time interval τ between two microwave pulses with turning angles $\pi/2$ and π to generate an echo envelope that maps the time course of relaxation of the spin system (in ESEEM) or as a function of the magnetic field at fixed τ (in field-sweep ESE). In the two-dimensional (2D) four-pulse ESEEM experiment ($\pi/2 - \tau - \pi/2 - t_1 - \pi - t_2 - \pi/2 -$echo), also called HYSCORE [15], the intensity of the stimulated echo after the fourth pulse is measured with t_2 and t_1 varied while τ is constant. Such a 2D set of echo envelopes gives, after complex Fourier transformation, a 2D spectrum with equal resolution in each direction. Spectral processing of ESEEM patterns was performed using Bruker WIN-EPR software, including subtraction of the relaxation decay (fitting by 3–6 degree polynomials), apodization (Hamming window), zero filling, and fast Fourier transformation.

Pulsed ENDOR spectra of the radicals can be obtained using Davies ($\pi - t - \pi/2 - \tau - \pi - \tau -$ echo) [16] and Mims ($\pi/2 - \tau - \pi/2 - t - \pi/2 - \tau -$ echo) [17] microwave sequences with different pulse lengths. In addition, radiofrequency π pulse is applied during the time interval t in both sequences. The individual characteristics of each ESEEM/ENDOR experiment are provided in figure captions. In this work, we made Davis ENDOR and compared it with Mims ENDOR data from another laboratory.

3 Results

3.1 EPR Spectra of Dried $TiO_2 + H_2O_2$ Sample

A dried sample of TiO_2 (solution of $Ti(OiPr)_4$ treated with H_2O_2, the suspension was placed under vacuum immediately after preparation) (sample I) shows characteristic signal with rhombic g-tensor in X and Q-band EPR spectra recorded at temperature 90 K (Fig. 1). The g-tensor principal components measured from Q-band spectrum are $g_{zz} = 2.0236$, $g_{yy} = 2.0082$, and $g_{xx} = 2.0015$. This result strongly suggests the presence of a stable superoxide radical anion generated by the decomposition of H_2O_2 on the TiO_2 surface [10]. The g_{zz} values in the range between 2.019 and 2.026 are usually reported for superoxide on TiO_2 surfaces (see Table 1), which are consistent with those expected for $O_2^{\bullet -}$ stabilized at Ti^{4+} site ($O_2^{\bullet -}$-Ti^{4+}) [5]. The $^1H/^2D$ exchange in the sample influences only slightly a width of the spectral components (Figure S1).

3.2 Pulsed EPR Characterization of the Superoxide

Interaction of the paramagnetic species with the environment in the sample I was probed using pulsed ENDOR and 2D ESEEM (HYSCORE). Q-band Davies

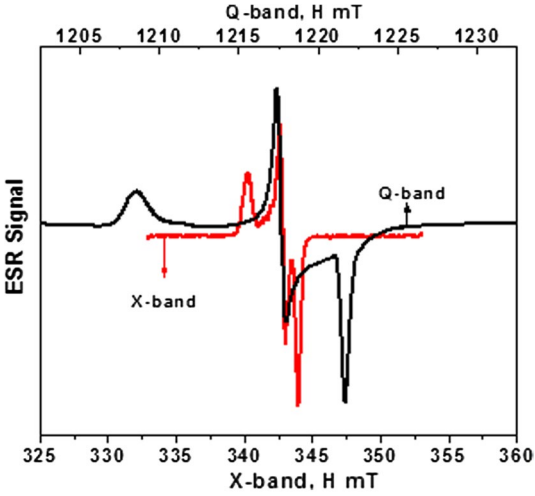

Fig. 1 X (grey) and Q-band (black) EPR spectra of superoxide radical in sample I obtained as a first derivative of field sweep two-pulse ESE patterns. Experimental parameters: $\pi/2$ and π pulse length 100 and 200 ns, time between first and second pulses $\tau = 400$ ns, microwave frequency 9.6352 GHz (X-band) and 34.1914 GHz (Q-band), and temperature 90 K

Table 1 g-tensors assigned to $O_2^{-\bullet}$ radical in different TiO_2 samples

Matrix	g_{zz}	g_{yy}	g_{xx}	Reference
$Ti(OiPr)_4/H_2O_2$	2.0235	2.0093	2.0033	10
TiO_2 (rutile) 30 wt% H_2O_2 60 wt% H_2O_2	2.025[a,b] 2.021[b]	2.009 2.009	2.003 2.003	18
Ti-anatase (H_2O_2-treated)	2.025	2.011	2.0034	19
Ti gel prepared from metallic Ti powder and 10 M H_2O_2	2.023 2.025 2.021	2.009 2.009 2.009	2.003 2.003 2.003	20
$Ti(OiPr)_4/H_2O_2$	2.0227[c] 2.024[d]	2.0074 2008	2.0010 2.002	This work
TiO_2 (P25)	2.019 2.020 2.023 2.026	2.011 2.011 2.011 2.011	2.005 2.004 2.004 2.001	21,22
TiO_2 on porous Vycor glass	2.0268	2.0088	2.0036	4
Dehydrated Pt/TiO_2 photo catalysts (PT-1 and PT-2)	2.021 2.022	2.008 2.007	2.000 2.001	23
TiO_2 (millennium PC500, mesoporous)	2.0288	2.009	2.0037	24
Dye-sensitized TiO_2	2.0253	2.009	2.0031	25
Reduced TiAlPO-5	2.023	2.010	2.003	26

[a]30 wt% H_2O_2

[b]60 wt% H_2O_2

[c]Q-band

[d]X-band

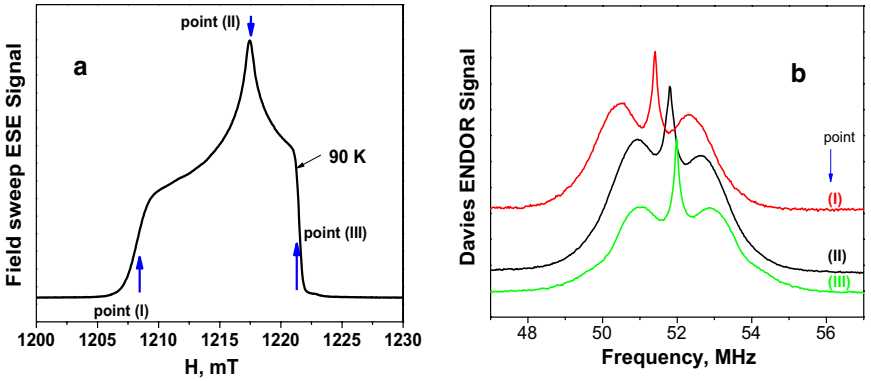

Fig. 2 Q-band field-sweep 2-pulse ESE spectrum (**a**) and Q-band Davies ENDOR spectra (**b**) of the superoxide radical in sample I. The microwave frequency was 34.2198 GHz, $\pi/2$ pulse = 100 ns, the magnetic field was set to 1208.0 mT (I), 1217.4 mT (II), 1221.5 mT (III), and the temperature was 90 K

ENDOR spectra collected at magnetic fields of the EPR spectrum corresponding to principal values of the *g*-tensor of the superoxide in sample I (points I – III, Fig. 2a) show the narrow matrix peak at the proton Zeeman frequency with two broad symmetrically located shoulders (Fig. 2b). The splitting between the maxima of the shoulders in all three spectra varies within 2.1 ± 0.1 MHz.

X-band HYSCORE spectra obtained for this sample show ^{1}H signal located around diagonal point (ν_{1H}, ν_{1H}) and changing its shape with the variation of time τ between first and second pulses. At $\tau = 120$ ns the signal possesses an intensive peak located around the diagonal point (ν_{1H}, ν_{1H}) with extended shoulders (Figure S2). On the other hand, at $\tau = 200$ ns the intensity at the diagonal point is completely suppressed and two well-separated cross-features 1_H oriented along (ν_{1H}, ν_{1H}) antidiagonal are observed (Fig. 3a and S3). In addition, both spectra show diagonal low frequency peaks at 1.56 and 2.25 MHz. In the sample similarly prepared using D_2O_2, very intensive signal appears at the frequency ~2.25 MHz, which corresponds to the ^{2}D Zeeman frequency in the applied magnetic field. Accordingly, the intensity of ^{1}H signal was suppressed, indicating the replacement of a significant part of the exchangeable protons from H_2O and OH groups in the superoxide radical environment by deuterium nuclei ^{2}D (Fig. 3b and S3).

Low and high intensive peaks located at the frequency 2.25 MHz of the diagonal line in the spectra shown in Fig. 3a, b and S3 exhibit similar lineshape. The intensive ^{2}D peak (Fig. 3b) consists of two halves splitted on ~0.2 MHz along the diagonal by the quadrupole interaction of the deuterium. The weak signal in Fig. 3a possesses exactly the same lineshape with similar splitting and can only be produced by the ^{2}D nuclei contained with the natural abundance (0.0115%) in the sample I prepared using H_2O_2. The clear observation of this peak was probably made possible due to very high signal-to-noise ratio in these spectra.

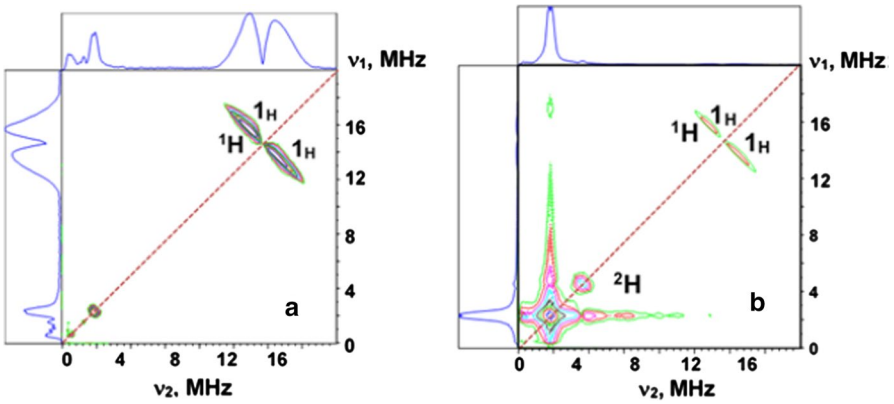

Fig. 3 Contour representation of the HYSCORE spectra of superoxide radical in the sample I (**a**) and in the similar sample prepared using D_2O_2 (**b**). The time τ, between the first and the second microwave pulses, was 200 ns. The spectrum was obtained by FT of the 2D time-domain patterns containing 256×256 points with a 16 ns step in t_1 and t_2, which are the intervals between the second and the third microwave pulses, and the third and the fourth microwave pulses, respectively. 3D-type stacked presentations of these spectra are shown in Figure S3. The microwave frequency was 9.635 GHz (**a**) and 9.6342 (**b**), and the magnetic field was set to 342.9 mT (**a**) and 342.85 mT (**b**), and the temperature was 90 K

4 Discussion

4.1 Analysis of the ^{1}H HYSCORE and pulsed ENDOR spectra

Quantitative analysis of the ^{1}H cross-ridges from HYSCORE spectra of $O_2^{-\bullet}$ in samples I, based on a linear regression of contour lineshapes in ν_1^2 *vs* ν_2^2 coordinates [27] (see Figure S4 and Table S1), provides the isotropic and anisotropic components of the hyperfine tensors under an axial approximation for the proton(s) interacting with superoxide's electron spin. Detailed explanations of the analysis are described in the Supporting Info and the complete results of the analysis are shown in Table S1. Particularly the analysis of cross-ridges 1_H from the spectra of sample I prepared with H_2O_2 and D_2O_2 gives anisotropic hyperfine coupling $T = 2.0 \pm 0.2$ MHz for the contributing proton(s) and also points at a possible presence of a small isotropic coupling of ~1 MHz. In the HYSCORE spectrum, two characteristics can provide quantitative information about anisotropic coupling T. One is the total length of the cross-ridge equal to $3T/2$ if entire ridge is observed. The other is a maximum deviation of the cross-ridge from antidiagonal crossing the diagonal at (ν_{1H}, ν_{1H}) point. The deviation of the cross-ridges from the diagonal in the experimental spectra is negligible, supporting the estimated value of T~2 MHz and the corresponding O–H distance > 3 Å (see next section). The presence of an isotropic coupling for such distances without a stable atomic bridge enabling a spin delocalization through chemical bonds would be very unusual. This HYSCORE analysis was based on a single proton interaction. In addition, there is a strong and wide matrix line in the spectra recorded at $\tau = 120$ ns (Figures S2b). As a result, the cross-ridges observed in the spectra with the suppressed ^{1}H diagonal intensity

(Fig. 3a,d) may still contain contributions from the matrix peak, which can influence the results of the HYSCORE analysis.

For comparison, Q-band Davies ENDOR spectra collected at magnetic fields of the EPR spectrum corresponding to principal values of the *g*-tensor of the superoxide in sample I (points I – III, Fig. 2a) show the narrow matrix peak at the proton Zeeman frequency with two broad symmetrically located shoulders (Fig. 2b). The splitting between the maxima of the shoulders in all three spectra varies within 2.1 ± 0.1 MHz that is consistent with the value of anisotropic coupling determined from the HYSCORE spectra. Unfortunately, the excessive broadening of the ENDOR lines does not allow one to obtain a direct estimate of *a* and *T* components of the hyperfine tensor. However, the proton hyperfine interaction in our case cannot be purely isotropic, because then ESEEM would not be observed at all.

The same value of $T \sim 2$ MHz was determined from the ^{1}H X-band Mims ENDOR spectra of the superoxide anion at Ti^{4+} site in TiAlPO-5 [26] and assigned to a proton located at the distance 3.4 Å from $O_2^{\bullet-}$ estimated using point dipoles approximation. Similarly to our case, spectra recorded at field settings corresponding to the principal values of the *g*-tensor lack features typical for well-pronounced orientation selection but the splitting of ~2 MHz is only observed in the spectrum recorded at g_{xx} field position (Figure S5). A significant individual line-width (0.75 MHz) explained by a conformational heterogeneity in the polycrystalline sample was used in simulations of the ENDOR spectra in [26].

Our preliminary ENDOR simulations show that the experimental spectra can be reproduced by the interaction of superoxide with a proton possessing an anisotropic hyperfine tensor with $T = 2$ MHz, which can acquire different orientations with respect to the g-frame. For simplicity, we have modeled this distribution with two orientations implemented with relative statistical weights.

This result allows us to suggest that even the nearest protons surrounding the superoxide radical in these samples fail to form any regular structure and are randomly distributed at distances that satisfy the condition where $T \approx 2$ MHz. Therefore, the development of the model describing the lineshape of the orientation-selective ENDOR spectra with the similar splitting of the resolved components for more complex distributions of the proton environment, needs more deep computational analysis.

4.2 Evaluation of the proton anisotropic hyperfine couplings

The value of $T \sim 2$ MHz for superoxide-proton coupling discussed above is significantly smaller than previously reported ^{1}H hyperfine couplings of $T \sim 10$ MHz determined from HYSCORE spectra of the superoxide species generated on sodium precovered MgO surface [28] and produced in reaction of KO_2 with water in DMSO/H_2O solution in the presence of ubiquinone-10 [29]. The anisotropic hyperfine interaction with the proton located near the superoxide ion results from the dipole–dipole interaction with unpaired spin density delocalized approximately equally over two oxygens separated by just one bond length. The local magnetic field induced at the proton by the spin density distributed over two oxygens would depend on its location

relative to the O–O bond and generally represented by the rhombic hyperfine tensor [30]. The magnitude of anisotropic dipole − dipole interaction T between the spin of the unpaired electron and the spin of the coupled proton is defined by the distance r between them as $1/r^3$. In the point dipole approximation, $= \frac{g_e g_I \beta_e \beta_I}{hr^3}$, where g_e, g_I, β_e, and β_I are the respective electronic and proton nuclear g-factors and magnetons, and $T = \frac{79}{r^3}$(MHz) for proton. The dipole–dipole interaction depends on the magnetic field direction and is described by axially symmetric tensor with diagonal principal values

$$\boldsymbol{T} = \left[T_{xx} \cdot T_{yy} \cdot T_{zz}\right] = T \cdot [-1, -1, 2] \tag{1}$$

in the principal axes coordinate system with **z** axis directed along $\vec{r}$ direction.

The proton located near a superoxide with the oxygens O_1 and O_2 carrying unpaired spin densities ρ_1 and ρ_2 experiences a dipolar interaction that depends on the O_1–H distance (r_1) and the O_2–H distance (r_2) (Figure S6). The spin densities ρ_1 and ρ_2 produce local magnetic field on the proton, which is a vector sum of these two contributions. Generally, hyperfine tensor in this case is rhombic as followed from the formula defining hyperfine tensor for proton interacting with separated arbitrary electron spins [30]. The principal values of the resulting hyperfine tensor adapted to our case are

$$\boldsymbol{T} = \left[\tfrac{1}{2}\left(T_1 + T_2 - 3\delta\right), -\left(T_1 + T_2\right), \tfrac{1}{2}\left(T_1 + T_2 + 3\delta\right)\right] \tag{2}$$

where $\delta = [{T_1}^2 + {T_2}^2 + 2T_1T_2\cos(2\alpha + 2\beta)]^{1/2}$, $T_1 = 79\ \rho_1/{r_1}^3$, $T_2 = 79\ \rho_2/{r_2}^3$. For the angle $\beta = 180°$, when the proton lies on the O_1–O_2 line, $\delta = T_1 + T_2$ and (Eq. 2) for tensor T transforms to traditional axial form.

$$T = \left[-\left(T_1 + T_2\right), -\left(T_1 + T_2\right),\ 2\left(T_1 + T_2\right)\right] \tag{3}$$

The geometric relations between the sides and angles of the triangle HO_1O_2 (Figure S6)

$$r_2^2 = [r_1^2 + r_{O-O}^2 - 2r_1 r_{O-O}\cos\beta]^{1/2} \text{and } \alpha = \arcsin\left[\frac{r_1}{r_2}\sin\beta\right] \tag{4}$$

allow for the definition of the tensor components based on one distance (r_1) and one angle (β).

In the case of superoxide radical, the added electron is almost equally distributed on the two O atoms in solution [31]. Similarly, the unpaired spin density on $2p_\pi^{\ x}$ of each oxygen is ~0.495 in $O_2^{\bullet-}$ adsorbed on MgO surface as shown in experiments using magnetic isotope ^{17}O [32]. Magnetically equivalent ^{17}O oxygens have also been reported for $O_2^{\bullet-}$ generated in TiAlPO-5 [26]. The reported distance between the oxygens in superoxide varies within 1.32–1.35 Å [31,33–35] and increases in the presence of hydrogen bonds [31, 33].

For direct comparison with the experimental values $T = 2$ (this work) and 10 MHz [28, 29] determined form the HYSCORE analysis in the axial approximation, we selected term $T_1 + T_2$ from Eq. 2, which lacks the rhombic term 3δ, and is equal

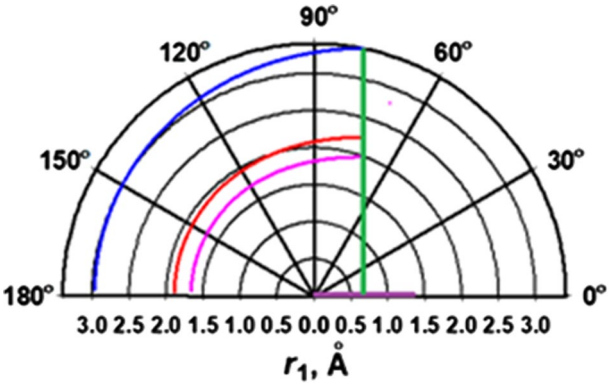

Fig. 4 Polar graphs (r_1, β) with representative contours $T = 39.5\,[\frac{1}{r_1^3} + \frac{1}{r_2^3}]$ equal to 2.0, 7.0, and 10 MHz calculated for a model with one superoxide oxygen located in the (0, 0) point of coordinates and second oxygen in the point (1.33 Å, 0°). O_1–O_2 distance equals to 1.33 Å along the line with $\beta = 0°$. Line normal to r_1 axis corresponds to the middle of the O_1–O_2 distance (see also Table 2)

Table 2 Distances of a proton location relative to a superoxide radical at different values of the anisotropic hyperfine coupling

T, MHz	r_1 (H–O_1), Å	β, degree	r_1 at $\beta = 180°$, Å	r_1 at $\beta = 120°$, Å
2	2.97–3.4	180–75	2.97	3.08
7	1.89–2.24	180–73	1.89	1.95
10	1.67–1.99	180–70	1.67	1.71

$T = 39.5\left[\frac{1}{r_1^3} + \frac{1}{r_2^3}\right]$ for $\rho_1 \approx \rho_2 \approx 0.5$. It was calculated in the form of contours, where each point defines r_1 and β with selected T (2, 7, or 10 MHz) (Fig. 4), i.e. as a function of the O_1-H distance between the proton and nearest oxygen of $O_2^{\bullet-}$ at the angle β between H–O_1 and O_1–O_2 directions. The coupling with $T \sim 7$ MHz is included in our analysis as an example demonstrating variation of distances at an intermediate value of T. Calculated graphs show that $T = 2$ MHz corresponds to the distance 2.97 – 3.4 Å between H and nearest O_1 for the angles $\beta < 180°$ between O_1-H and O_1-O_2 (Table 2). In contrast, this distance is ~1.0–1.2 Å shorter for $T = 7$ or 10 MHz (Table 2).

Existing models of a hydration shell for the aqueous $O_2^{-\bullet}$ include four water molecules with two waters forming hydrogen bonds with each oxygen atom (Figure S7). The hydrogen bond lengths reported for the structures predicting the O–O bond length within the limit 1.336 (±0.005) Å and positive the vibrational frequency shift on solvation of the radical varies within 1.72–1.94 Å [31, 36, 37]. Lower limit of H-O_1 distance estimated for $T = 7$ MHz is still within the indicated interval.

In the limiting case of unpaired electron localization on one oxygen, the O–H distances corresponding to $T = 2$, 7, and 10 MHz are equal 3.4, 2.24, and 1.99 Å, respectively, that corresponds to estimates using a point dipoles approximation. One

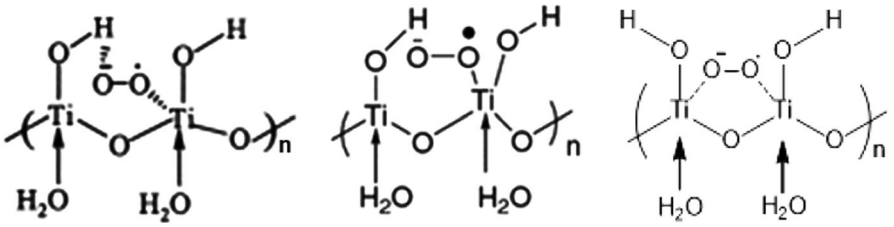

Fig. 5 The proposed structure of titanium superoxide in $Ti(OiPr)_4$ catalyst exposed to H_2O_2. (left, **a**) from ref.10. Adapted by permission from Copyright Clearance Center: John Wiley and Sons, Dewkar et al. [10]. Copyright 2001. (center, **b**) from ref.12. Adapted by permission from Copyright Clearance Center: Springer Nature, Reddy et al. [12]. Copyright 2010. (right, **c**) this work

can note that for the spin density equally distributed between two atoms in $O_2^{-\bullet}$ radical, the distances between H and each oxygen are equal to a point dipole estimate when the proton is located on the line of the symmetry normal to the central point of the O–O bond.

4.3 Models of $O_2^{\bullet -}$ radical interaction with the catalyst environment

The discussed catalyst with superoxide species on the hydrated titanium matrix has been thoroughly examined by various spectroscopic techniques [10]. Its IR spectrum showed characteristic absorption bands assigned to vibrational modes of coordinated water molecules at Ti^{4+} site (3720 and 3665 cm^{-1}) and of surface Ti–OH groups (3450 cm^{-1}). Additional IR bands in the range of 900–538 cm^{-1} and an intense line at 900 cm^{-1} in the Raman spectrum confirmed the presence of Ti–O–Ti linkages in the catalyst. The IR absorption bands 1027 and 1157 cm^{-1} and weak Raman lines observed in the range of 1025–1119 cm^{-1} were assigned to $O_2^{\bullet -}$ in the solid matrix. The X-ray diffraction pattern did not show any sharp peaks, thus indicating its amorphous nature of $Ti/O_2^{\bullet -}$ catalyst. The formation of the superoxide radical was also confirmed by the EPR spectrum with the characteristic principal values of the g-tensor (Table 1).

These results were illustrated by the proposed model of the $O_2^{\bullet -}$ stabilization on titanium superoxide catalyst shown in Fig. 5a [10]. This model does not provide any geometrical characteristics and suggest the location of one oxygen near Ti^{4+} and the second oxygen interacts with the proton of –OH group coordinating the neighboring Ti. Slightly different image of this structure was shown in the review article [12] from the same group accompanied by the similar text as in [10] (Fig. 5b).

There are a number of publications describing an EPR characterization of the superoxide in different H_2O_2 treated titanium samples (4 rows from the top in Table 1). All of them report the species with very similar *g*-tensors, which can be assigned to the $O_2^{\bullet -}$ stabilized near Ti^{4+} although reported spectra were recorded at different temperatures, i.e. at room temperature [10, 12] and [20], at 77 K [19], and at various temperatures [18] and at 90 K in this work.

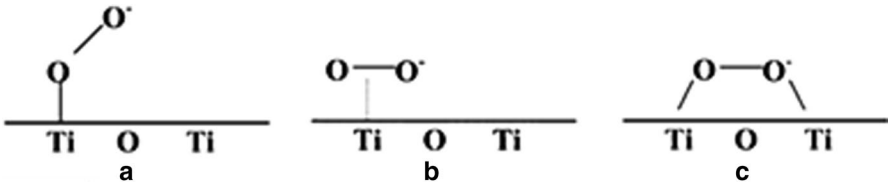

Fig. 6 Suggested models of superoxide – Ti coordination on TiO_2 surface. The interaction with a metal is classified as "end-on" or "side-on" to indicate the connection as η^1 (one atom bound to the metal) or η^2 (two atoms bound to the metal), respectively. These models correspond to "end-on" (**a**), side-on (**b**), and "end-on/end-on" or "bridging superoxo" coordination (**c**). Adapted from Ref. 18 with permission from the PCCP Owner Societies

The hydrogen peroxide treated polycrystalline titanium oxide systems (TiO_2, TS-1, [Ti]-APO-5 and ion-exchanged Ti-ZSM-5) have been investigated using X-band EPR [18]. Two orthorhombic EPR signals with g_{zz} values of 2.025 and 2.0215, assigned to adsorbed $O_2^{\bullet -}$ anions, were found in the TiO_2 (rutil phase)/(30 or 60 wt%) H_2O_2 system [18]. The superoxide with $g_{zz}=2.025$ was observed for either H_2O_2 concentration. Species with smaller g_{zz} components were only resolved in 60 wt% H_2O_2/TiO_2 (Table 1), which suggests the presence of two different environments for $O_2^{\bullet -}$ radical stabilization at a Ti^{4+} site [5]. The changes in the g_{zz} values were interpreted as the existence of variously coordinated $Ti(O)_n$ centers and three different models of superoxide coordination with Ti (Fig. 6).

The EPR spectra of the 60 wt% H_2O_2-treated samples, after evacuation at room temperature, were measured at temperatures between 10 and 230 K. They revealed that the spectral lines do not undergo any shifts as a function of temperature, while only limited line broadenings occur at temperatures above 50 K. The component with $g_{zz}=2.025$ possesses stronger broadening compared to the $g_{zz}=2.0215$ one and, thus, supports the hypothesis that there are heterogeneity between the two $O_2^{\bullet -}$ species.

The article [18] cited the work by Dewkar et al. [10] as an example of an exceptionally stable titanium superoxide radical ion formed in the homogeneous phase that excluded any possibility for a heterogeneous environment for the titanium ions. It was also proposed that a low-coordinated $Ti(O)_3OO^{\blacksquare}$ species produce a superoxide-like EPR spectrum with $g_{zz}=2.0235$ [18]. The EPR spectrum of dried $TiO_2+H_2O_2$ sample in [10, 12] was collected at room temperature (298 K). The spectrum possesses pure powder-type lineshape without any effects indicating radical mobility. One can note, however, that the g_{zz} component of this spectrum has an asymmetric shape with the shoulder at high-field side, which can be interpreted as a formation of two different species with g_{zz} equals to 2.0235 and 2.0217 (Figure S8). Those are close to g_{zz} values reported for two superoxide species observed in H_2O_2 treated TiO_2(rutile) [18]. Nevertheless, this spectral feature was ignored by the authors of refs. 10,12 and 18.

In contrast, our X and Q-band spectra of the similarly prepared sample show symmetrical g_{zz} line (Fig. 1) and assumes the formation of just one type of $O_2^{\bullet -}$ species. Our only difference with [10] is the use of 30 wt% H_2O_2 instead of 50% wt H_2O_2,

i.e. one can suggest a larger amount of adsorbed water in our sample after its evacuation at room temperature. Qualitatively, our finding is consistent with the difference observed between 30 wt% and 60 wt% H_2O_2/Ti(rutil) samples in [18] (Table 1). The existence of exchangeable protons from H_2O or OH weakly coupled with superoxide is verified by the intensive line appeared around the diagonal point (ν_{2D}, ν_{2D}) in the HYSCORE spectrum of the sample I prepared with $^2D_2O_2$ that is also accompanied by the intensity loss of ^1H lines (Figs. 3, S3). However, our pulsed EPR data does not indicate any specific $O_2^{\bullet -}$…H interactions consistent with H-bond formation requiring typical O–H distances <2 Å. Analysis of the cross-peak lineshape assuming interaction with a single nucleus gives effective value of anisotropic coupling $T \sim 2$ MHz corresponding to distances 2.97–3.4 Å (Table 2).

The X-ray diffraction pattern indicates amorphous nature of Ti/$O_2^{\bullet -}$ catalyst [10, 12]. Due to existing uncertainties with bulk modules in the H_2O_2-treated TiO_2 catalyst, one can consider possible geometry of the superoxide interaction with TiO_2 surface using the models of local interaction with surface Ti ions [18] as shown in Fig. 6. For these purposes, one can briefly describe characteristic geometry of TiO_2 structures examined in the literature. Computational works have found that the lowest-energy geometry of a TiO_2 molecule is a bent structure with a Ti–O distance of 1.63–1.65 Å and a bond angle near 111°. A symmetric linear conformer was also found on the ground state potential surface but was attributed to a saddle point rather than a true minimum [38, 39]. Ti–O distance in a linear structure is 1.699 Å [39]. Anatase and rutile surfaces are the two major TiO_2 polymorphs [40]. Parameters optimized crystal structures of rutile (110) and anatase (101) reported in [39] (Ti – O distances 1.96 Å in rutile and 1.95 and 2.01 Å in anatase) are in good agreement with available experimental data [41]. O – Ti – O angles in rutile are either 90 or 180° and in anatase they are around 77, 102, and 180° [39]. DFT studies of Ti^{4+} hydroxides and their clusters with expanded titanium coordination reported Ti–O and O–H distances of 1.80 ± 0.02 Å and 0.96 ± 0.01 Å, respectively, and Ti–O–H angle of 100–180° for Ti–OH fragment [42]. Calculations of $Ti(OH)_4$ complex gives the Ti–O distance of 1.88 Å and Ti–O–H angle of 119.0°[43].

DFT calculations were also performed for side-on adsorption (structure b) on anatase (101) and rutile (110) surfaces of TiO_2. The results showed slight differences in both bond lengths and adsorption energies between the two surfaces (Figure S9). Particularly, Ti–O distances with two superoxide oxygens and the length of O–O bond in $O_2^{\cdot -}$ were 2.036, 2.029 and 1.331 Å in anatase, and 1.955, 1,881 and 1.48 Å in rutile [44]. However, the calculations in this work were performed for ideal surfaces without any adsorbed molecules.

The model proposed in [10, 12] (Fig. 5) suggests that the superoxide is located near two surface Ti atoms coordinated with OH groups. Using the structural characteristics provided above, one can estimate the distances between the superoxide oxygen O_s and nearest proton of the OH group for structures a-c (Fig. 6) assuming that $O_2^{\cdot -}$ and –OH are coordinated to two neighboring titanium atoms.

For a Ti–O bond of 1.95–2.0 Å, the largest distance between Ti atoms in the fragment Ti–O-Ti is equal ~3.9–4.0 Å at the bent angle 180°. This distance decreases at smaller angles. For instance, it is ~3.38–3.46 Å for the angle 120°. This estimate indicates that the O_s…H distance ~3.0 – 3.5 Å in the structure a is only possible

at the bent angles of Ti–O_s–O_s and Ti–O–H groups > 160–170°. In structure b the smallest distance O_s…H ~ 3 Å could be obtained for the bent angle of Ti–O–H ≥ 150°. These estimates were obtained with an assumption that O_s and H are located in the same plane with coordinated Ti atoms. Any deviation of O_s or H from this plane would increase the estimated distance between them.

Structure *c* of bridging superoxide coordination to two titaniums is more complex where Ti–O–Ti and Ti − O_s–O_s–Ti bridges are not located on the same plane (Figure S10) [45]. Our estimates show that O_s…H distance ≥ 3 Å that satisfies the experimental finding $T = 2$ MHz is only possible when the proton of the O–H group, bound to one of the bridged Ti, is oriented in the direction opposite to O_s–O_s (Figure S10) and is not suitable for the formation of any bond shown in Fig. 5. Thus, this simple analysis suggests that structures (b) and (c) are more appropriate for the explanation of the small ^{1}H hyperfine couplings between the superoxide and the nearest protons. These estimates correlate with the conclusion that the $O_2^{\bullet -}$ …H distance 3.4 Å derived from the coupling $T = 2$ MHz in TiAlPO-5 is only consistent with the presence of an OH^- group in the second oxygen coordination sphere of the side-on adsorbed $O_2^{\bullet -}$ – Ti^{4+} center [26].

Additional arguments for the selection of the preferred coordination structure of superoxide in the studied catalyst can be obtained considering the lack of superoxide mobility even at room temperature. In the case of end-on unidentate coordination of a superoxide (a) to the Ti^{4+}, a rotation about the Ti–O bond would be expected to occur at temperatures even below room temperature. It would lead to characteristic averaging of the g-tensor components and spectral transformation from rhombic to axial lineshape [18, 46]. However, the lineshape and g-tensor of EPR spectrum reported for the superoxide in [10, 12] are similar to these characteristics observed at low temperatures in other H_2O_2 treated TiO_2 samples (Table 1) that excludes any rotational mobility. In addition, this geometry allows minimum distances of < 2 Å between the noncoordinated oxygen of $O_2^{\bullet -}$ and protons of O–H group from neighboring Ti, thus it enables the formation of H-bonds with ^{1}H hyperfine coupling stronger than 2 MHz. The motional averaging in the EPR spectra of side-on bidentate adsorbed superoxide (structure b) have also been observed at low temperatures and studied in detail [18, 47, 48]. This argument does not allow us to consider this structure as preferable despite the observation of similar proton coupling $T = 2$ MHz for side-on adsorbed superoxide in TiAlPO-5 [26].

The IR absorption bands 1027 and 1157 cm^{-1} and weak Raman lines observed in the range of 1025–1119 cm^{-1} were assigned to $O_2^{\bullet -}$ in the solid matrix of Ti/$O_2^{\bullet -}$ catalyst [10, 12]. Lever et al. [49] have previously suggested that O–O stretching frequencies in the range 1075–1195 cm^{-1} are indicative of superoxo-like dioxygen adducts (Fig. 6c). One can expect that the rigidity of the η^2 bound complex would prevent easy rotation of the anion and exclude significant *g* tensor averaging of g_{zz} and g_{xx} components observed in the EPR spectra of side-on coordination b.

In addition to magnetic ^{1}H nuclei, the catalyst contains magnetic isotopes of titanium, ^{47}Ti ($I = 5/2$, 7.44%, $g_n = -0.31484$) and ^{49}Ti ($I = 7/2$, 5.41%, $g_n = -0.31491$). Our HYSCORE spectra do not show any features that could be assigned to these nuclei. The cross-lines assigned to ^{47,49}Ti were observed in HYSCORE of open-shell Ti^{3+} ions generated in hybrid SiO_2–TiO_2 mesoporous monoliths [50]. The

spectrum recorded at the $g_{\|}$ position contains cross-peaks from ^{47,49}Ti corresponding to the hyperfine coupling of ~6 MHz. Signals from ^{47,49}Ti were not detected in spectra collected at other field orientations in the g-tensor frame due to the significant increase in hyperfine coupling. This result is in line with experimental [51–53] and theoretical [54] studies of ^{47,49}Ti hyperfine couplings in beryl single crystals. Results of [51–54] are consistent with each other and report $A_{\|}$~0–2 G (0–6 MHz) and $A_{\perp}$ ~18–20 G (50–56 MHz) for both ^{47,49}Ti isotopes. It defines the substantial isotropic constant of the order 12–13 G (33–37 MHz). The values of $A_{\perp} = 52.6 \pm 0.2$ MHz have been reported for ^{47,49}Ti in the mixed sandwich compounds of Ti^{3+} [55]. The DFT calculations of the valence electron density of neutral and cationic Ti species show a very low population at the nucleus in Ti^{3+} in contrast with Ti^{0}-Ti^{2+} states [39]. These values of couplings allow one to suggest that the transfer of spin density from superoxide electrostatically adsorbed in either "end-on" or "side-on" position on Ti^{3+} would not be sufficient for creation of hyperfine couplings of ~5–10 MHz, leading to the appearance of the observable cross-peaks from ^{47,49}Ti in HYSCORE spectra.

5 Conclusion

The superoxide anion stable at room temperature, generated by treating $Ti(OR)_4$ (R = iPr, nBu) with H_2O_2, was reported and used as a selective heterogeneous catalyst for the oxidation of organic compounds [10]. It was proposed that exceptional stability of the radical is resulted from its stabilization near Ti^{+4} cation on the TiO_2 surface with the participation of water molecules and/or OH groups. In this article, we performed pulsed EPR study on the superoxide radical in this catalyst with the aim to obtain quantitative information about $O_2^{\bullet -}$ interactions with the surrounding molecules. Our HYSCORE and pulsed ENDOR data have shown that the $O_2^{\bullet -}$ is involved in weak hyperfine interactions with protons in the nearest environment. Anisotropic coupling of the radical with proton(s) does not exceed a value of 2 MHz, corresponding to O_s…H distances $\geq$3 Å that exclude the formation of H bonds. The analysis of possible structures of $O_2^{\bullet -}$ adsorption on TiO_2 surface, taking into account our results and lack of radical mobility at room temperature observed in EPR spectra [10], led us to suggest that $O_2^{\bullet -}$ is stabilized in the form of superoxo bridge coordinated with two titanium atoms (Fig. 5c). Further support for this model can be obtained from the EPR experiments with ^{17}O labeled superoxide, which can provide information about the distribution of unpaired spin density over two oxygen atoms and accompanying calculations of electronic structure for different coordination models.

Supplementary Information The online version contains supplementary material available at https://doi.org/10.1007/s00723-021-01424-0.

Acknowledgements This work was supported by Grant DE-FG02-08ER15960 (S.A.D.) from the Chemical Sciences, Geosciences and Biosciences Division, Office of Basic Energy Sciences, Office of Sciences, U.S. Department of Energy. The authors are grateful to Dr. Andrei Astashkin (University of Arizona) for help in the preliminary simulations of orientation-selective pulsed ENDOR spectra and very useful

discussions. This article is dedicated to Professors Klaus Möbius and Kev M. Salikhov on the occasion of their 85th anniversary. Both of them have done outstanding contributions in the science of magnetic resonance. The authors of this article had the privilege of professional communications with Professor Salikhov as well as friendly discussions at the "coffee club" in the laboratory of Professor Yu. D. Tsvetkov during many years of his and our work in V. V. Voevodsky Institute of Chemical Kinetics and Combustion (Novosibirsk). Later we have always been receiving encouraging support and help from Kev Minullinovich at multiple stages of his multifaceted career.

References

1. M. Hayyan, M.A. Hashim, I.M. AlNashef, Chem. Rev. **116**, 3029 (2016)
2. I.B. Afanas'ev, Russ. Chem. Rev. **48**, 527 (1979)
3. D.T. Sawyer, J.S. Valentine, Acc. Chem. Res. **14**, 393 (1981)
4. M. Anpo, M. Che, B. Fubini, E. Garrone, E. Giamello, M.C. Paganini, Top. Catal. **8**, 189 (1999)
5. M. Che, A.J. Tench, Adv. Catal. **32**, 1 (1983)
6. A.I. Kokorin, in *Chemical Physics of Nanostructured semiconductors*. ed. by A.I. Kokorin, D.W. Bahnemann (CRC Press, Utrecht-Boston, 2003), p. 203
7. M. Chiesa, E. Giamello, M. Che, Chem. Rev. **110**, 1320 (2010)
8. K. Sobańska, A. Krasowska, T. Mazur, K. Podolska-Serafin, P. Pietrzyk, Z. Sojka, Top. Catal. **58**, 796 (2015)
9. E. Giamello, P. Rumori, F. Geobaldo, B. Fubini, M.C. Paganini, Appl. Magn. Res. **10**, 173 (1996)
10. G.K. Dewkar, M.D. Nikalje, I.A. Sayyed, A.S. Paraskar, H.S. Jagtap, A. Sudalai, Angew. Chem. Int. Ed. **40**, 405 (2001)
11. G.K. Dewkar, T.M. Shaikh, S. Pardhy, S.S. Kulkarni, A. Sudalai, Indian J. Chem. B **44**, 1530 (2005)
12. R.S. Reddy, T.M. Shaikh, V. Rawat, P.U. Karabal, G. Dewkar, G. Suryavanshi, A. Sudalai, Catal. Surv. Asia **14**, 21 (2010)
13. G.K. Dewkar, V.V. Thakur, S.A. Pardhy, A. Sudalai, S. Devotta, Process for conversion of phenol to hydroquinone and quinones. US Patent 6872857. Date of Patent: Mar. 29, 2005
14. B.C. Benicewicz, S. Kanagasabapathy, A, Sudalai, Transition metal superoxides. US Patent 6765076. Date of Patent: Jul. 20, 2004
15. P. Höfer, A. Grupp, H. Nebenführ, M. Mehring, Chem. Phys. Lett. **132**, 279 (1986)
16. E.R. Davies, Phys. Lett. A **47**, 1 (1974)
17. W.B. Mims, Proc. Roy. Soc. A **283**, 452 (1965)
18. K.L. Antcliff, D.M. Murphy, E. Griffithsa, E. Giamello, Phys. Chem. Chem. Phys. **5**, 4306 (2003)
19. V. Ramaswamy, P. Awati, A.V. Ramaswamy, Top. Catal. **38**, 251 (2006)
20. P. Tengvall, I. Lundström, L. Sjöqvist, H. Elwing, L.M. Bjursten, Biomaterials **10**, 166 (1989)
21. J. Green, E. Carter, D.M. Murphy, Chem. Phys. Lett. **477**, 340 (2009)
22. E. Carter, A.F. Carley, D.M. Murphy, J. Phys. Chem. C **111**, 10630 (2007)
23. F. Liu, N. Feng, Q. Wang, J. Xu, G. Qi, W. Wang, F. Deng, J. Am. Chem. Soc. **139**, 10020 (2017)
24. V. Rahemi, S. Trashin, Z. Hafideddine, V. Meynen, S. Van Doorslaer, K. De Wael, Sens. Actuators, B Chem. **283**, 343 (2019)
25. J. Yu, J. Chen, C. Li, X. Wang, B. Zhang, H. Ding, J. Phys. Chem. B **108**, 2781 (2004)
26. S. Maurelli, M. Vishnuvarthan, G. Berlier, M. Chiesa, Phys. Chem. Chem. Phys. **14**, 987 (2012)
27. S.A. Dikanov, M.K. Bowman, J. Magn. Reson. Ser. A **116**, 125 (1995)
28. F. Napoli, M. Chiesa, E. Giamello, G. Preda, C. Di Valentin, G. Pacchioni, Chem. Eur. J. **16**, 6776 (2010)
29. R.I. Samoilova, A.R. Crofts, S.A. Dikanov, J. Phys. Chem. A **115**, 11589 (2011)
30. D.W. Randall, A. Gelasco, M.T. Caudle, V.L. Pecoraro, R.D. Britt, J. Am. Chem. Soc. **119**, 4481 (1997)
31. I. Janik, G.N.R. Tripathi, J. Chem. Phys. **139**, 014302 (2013)
32. M. Chiesa, E. Giamello, M.C. Paganini, Z. Sojka, D.M. Murphy, J. Chem. Phys. **116**, 4266 (2002)
33. P.D.C. Dietzel, R.K. Kremer, M. Jansen, J. Am. Chem. Soc. **126**, 4689 (2004)
34. H. Seyeda, M. Jansen, J. Chem. Soc. Trans. **6**, 875 (1998)
35. F. Halverson, J. Phys. Chem. Solids **23**, 207 (1962)
36. V.F. Antonchenko, E.S. Kryachko, Chem. Phys. **327**, 485 (2006)

37. V.F. Antonchenko, E.S. Kryachko, J. Phys. Chem. A **109**, 3052 (2005)
38. C.-K. Lin, J. Li, Z. Tu, X. Li, M. Hayashi, S.H. Lin, RSC Adv. **1**, 1228 (2011)
39. D. Koch, S. Manzhos, J. Phys. Chem. Lett. **8**, 1593 (2017)
40. M.E. Arroyo de Dompablo, A. Morales García, M. Taravillo, J. Chem. Phys. **135**, 054503 (2011)
41. D.T. Cromer, K. Herrington, J. Am. Chem. Soc. **77**, 4708 (1955)
42. I.S. Ignatyev, M. Montejo, J.J.L. González, J. Phys. Chem. A **111**, 7973 (2007)
43. S. Yin, D.E. Ellis, Phys. Chem. Chem. Phys. **12**, 156 (2010)
44. D. Wang, L. Zhao, D. Wang, L. Yan, C. Jing, H. Zhang, L.-H. Guo, N. Tang, Phys. Chem. Chem. Phys. **20**, 18978 (2018)
45. Y.-F. Li, A. Selloni, ACS Catal. **6**, 4769 (2016)
46. S. Schlick, L. Kevan, J. Am. Chem. Soc. **102**, 4622 (1980)
47. M. Shiotani, G. Moro, J.H. Freed, J. Chem. Phys. **74**, 2616 (1981)
48. R.F. Howe, W.C. Timmer, J. Chem. Phys. **85**, 6129 (1986)
49. A.B.P. Lever, G.A. Ozin, H.B. Gray, Inorg. Chem. **19**, 1823 (1980)
50. E. Morra, A. Budnyk, A. Damin, M. Chiesa, Top. Catal. **61**, 1485 (2018)
51. L.V. Bershov, J. Struct. Chem. **10**, 130 (1969)
52. D.R. Hutton, J.R. Pilbrow, G.J. Troup, J.O. Warne, Aust. J. Phys. **45**, 253 (1992)
53. V.P. Solntsev, A.M. Yurkin, Cryst. Rep. **45**, 128 (2000)
54. W.C. Zheng, Q. Zhou, X.X. Wu, Y. Mei, Z. Naturforsch. **61**, 286 (2006)
55. D. Courierand, E. Samuel, J. Am. Chem. Soc. **109**, 4571 (1987)